appreciation of the hospitality extended him by members of the Physics Department of New York University during the time when most of the work reported here was carried out.

*Work supported by the U.S. Atomic Energy Commission.

†Also Finch College, New York, N.Y. 10021.

‡Permanent address: Health Physics Division, Oak Ridge National Laboratory, Oak Ridge, Tenn. 37830 and Department of Physics and Astronomy, University of Tennessee, Knoxville, Tenn. 37916.

[1]E. Merzbacher and H. W. Lewis, Handb. Phys. **34**, 166 (1958).

[2]W. Brandt, in *Proceedings of the International Conference on Inner-Shell Ionization Phenomena, Atlanta, Georgia, 1972,* edited by R. W. Fink, S. T. Manson, M. Palms, and P. V. Rao (U.S. Atomic Energy Commission, Oak Ridge, Tenn., 1973), p. 948.

[3]G. Basbas, W. Brandt, and R. Laubert, Phys. Rev. A 7, 983 (1973).

[4]J. D. Garcia, Phys. Rev. A **4**, 955 (1971), and references cited therein.

[5]J. Bang and J. M. Hansteen, K. Dan. Vidensk. Selsk. Mat.-Fys. Medd. 31, (13) (1959).

[6]W. Brandt, R. Laubert, and I. Sellin, Phys. Rev. **151**, 56 (1966).

[7]N. F. Mott, Proc. Camb. Philos. Soc. **27**, 553 (1931). See also N. F. Mott and H. S. Massey, *The Theory of Atomic Collisions* (Clarendon, Oxford, England, 1965).

[8]D. R. Bates, H. S. Massey, and A. L. Stewart, Proc. R. Soc. Lond. A216, 437 (1953); D. R. Bates, Proc. R. Soc. Lond. A243, 15 (1957); D. R. Bates, Proc. R. Soc. Lond. A245, 299 (1958).

[9]This was first shown by Mott in Ref. 7 and has been invoked often as a proof that the Born approximation as applied to the calculation of charged-particle stopping power is valid for both $v_1/Z_2^* v_0$ very small and very large [M. S. Livingston and H. A. Bethe, Rev. Mod. Phys. **9**, 245 (1937)]. However, the proof in the limit $v_1/Z_2^* v_0 \ll 1$ applies only if $Z_1 \to 0$, as the present results show. The arguments are based on the assumption of a straight-line trajectory which, of course, is consistent with the limit $Z_1 \to 0$ and, hence, with the tenets of the PWBA (Ref. 3).

[10]G. Basbas, W. Brandt, and R. Laubert, Phys. Lett. A **34**, 277 (1971); and unpublished; W. Brandt, in *Proceedings of the Third International Conference on Atomic Physics, Boulder, Colorado,* 1972, edited by S. J. Smith (Plenum, New York, 1973), p. 155ff.

[11]G. Basbas, W. Brandt, R. Laubert, A. Ratkowski, and A. Schwarzschild, Phys. Rev. Lett. **27**, 171 (1971).

[12]A. R. P. Rau and U. Fano, Phys. Rev. **162**, 68 (1967).

[13]J. M. Hansteen and O. P. Mosebekk, Z. Phys. **234**, 281 (1970).

PHYSICAL REVIEW A VOLUME 7, NUMBER 6 JUNE 1973

Resonances in Photoelectron Angular Distributions*

Dan Dill

Department of Physics, The University of Chicago, Chicago, Illinois 60637

(Received 29 January 1973)

Photoelectron angular distributions should show pronounced variations with energy across autoionization resonances. This prediction applies quite generally to both atomic and molecular autoionization. Examples illustrate both the magnitude of the spectral variation and the inability of the Cooper-Zare model to account for the phenomenon. Calculations are reported for autoionization in xenon between the fine-structure levels $5p^5\ ^2P^o_{3/2}$ and $5p^5\ ^2P^o_{1/2}$ of the ion ground-state doublet. An analysis is given of the recent measurements by Niehaus and Ruf on autoionizing levels of the mercury Rydberg series $5d\ ^96s\ ^2(^2D)np$ and $5d\ ^96s\ ^2(^2D)n'f$ below the $Hg^+\ 5d\ ^96s^2\ ^2D_{5/2}$ threshold.

I. INTRODUCTION

The determination of the spectral variation of photoelectron angular distributions through autoionization resonances is a new and essentially untapped resource for photoelectron spectroscopy. Here this class of spectroscopic measurements is theoretically analyzed. The analysis predicts quite generally not only sharp spectral variations of the angular distributions across resonance features, but more importantly, angular distributions that should depart markedly from those predicted by direct (nonresonant) ionization models, such as the Copper–Zare model.[1] Deviations from direct ionization predictions arise owing to the enhancement by the autoionization process of the effects of just those forces that are often sufficiently weak as to go undetected in nonresonant photoionization. Accordingly, these resonances in photoelectron angular distributions are a sensitive new probe of photoejection dynamics.

This study rests on the angular-momentum-transfer formulation of angular correlations, given recently by Dill and Fano.[2] It also draws on extensive experience in analyzing the dynamical origin and significance of the various angular momentum transfers allowed in any given ionization process. This paper reports the most important implications and results for autoionization of the general dynamical analysis, whose full description is deferred to a separate report.[3]

Consider the schematic ionization process

$$A(J_0\pi_0)+\gamma(j_\gamma=1,\ \pi_\gamma=-1) \rightarrow A^+(J_c\pi_c)+e[ls\,j,\ \pi_e=(-1)^l]\ , \quad (1)$$

in which photoelectrons are ejected by electric dipole interaction from a generic unpolarized (atomic or molecular) target A. Dill and Fano (DF)[2] obtain a general expression representing the photoelectron angular distribution of process (1) in terms of separate components characterized by alternative magnitudes of

$$\vec{j}_t=\vec{J}_c+\vec{s}-\vec{J}_0=\vec{j}_\gamma-\vec{l}\ , \quad (2)$$

the angular momentum transferred in the ionization. The allowed values of $\vec{j}_t$ are those consistent with the balance of total angular momentum $\vec{J}$ and parity π,

$$\vec{J}=\vec{J}_0+\vec{j}_\gamma=\vec{J}_c+\vec{s}+\vec{l}\ , \quad (3)$$

$$\pi=\pi_0\pi_\gamma=\pi_c\pi_e =-\pi_0=(-1)^l\pi_c\ . \quad (4)$$

For any given ionization process, a range of j_t will be allowed, with ionization dynamics determining the relative contribution of different j_t components. However, each angular-momentum-transfer component has a characteristic angular distribution with an analytical structure independent of the dynamical details of the ionization. The predicted sharp variation of the angular distribution across resonance features follows from (a) the general structure of the distribution for each j_t, and (b) the spectral variation of the weights of distributions with different j_t. The deviations of the resulting angular distributions from predictions of direct ionization models, such as the Cooper–Zare formula,[1] follow from autoionization enhancing angular momentum transfers that can be unimportant in nonresonant ionization.[2,3]

Resonances in photoelectron angular distributions have already been calculated for the example of rotational autoionization in H_2 and the results show clearly the effects predicted here.[4] Additional examples will be given in this report. The specific examples have been chosen for their amenability to experimental verification: The resonances are wide and the spectral variations of the angular distributions are quite pronounced. Further, for both examples energy analysis of the photoelectrons is not required since only one group of photoelectrons is produced. Calculations are given for the angular distribution of xenon photoelectrons ejected into the autoionization region between the ionization thresholds of the $5p^5\,^2P^\circ_{3/2}$ and $5p^5\,^2P^\circ_{1/2}$ levels of the Xe^+ ground-state doublet. The results illustrate both a pronounced resonance in the angular distribution as well as substantial deviations from the predictions of the Cooper–Zare model.[1] The photoionization of mercury is analyzed in the resonant region between the $5d^{10}6s^2S_{1/2}$ level of ion ground state and the $5d^96s^2\,^2D_{5/2}$ level of the first excited state of Hg^+. This example is particularly striking: Since the ionization proceeds by an $s\rightarrow p$ transition, one might expect the photoelectrons to carry away the full anisotropy of the photon-target interaction, i.e., throughout the spectral region one might expect a fixed $\cos^2\theta$ angular distribution, peaking along the electric vector of the light. Actually, owing to the enhancement of spin-orbit effects in the resonant region, the analysis here predicts strong variations with energy which can extend over the full range from $\cos^2\theta$ to $\sin^2\theta$. Evidence of this sharp energy dependence of the Hg photoelectron angular distributions is seen in the recent measurements of Niehaus and Ruf.[5]

It is to be emphasized that a variety of dynamical interactions can result in multiple angular momentum transfers. In particular, *the forces are not restricted to just those of magnetic origin.*[2,3] Thus, in rotational autoionization of H_2, it is the torque exerted by the anisotropic *electric* field of the molecular ion that leads to parity-unfavored angular molecular transfer. For both the Xe and Hg examples, as we shall see, the anisotropy is provided by a combination of the *electrostatic* (exchange) interaction which separates different LS terms of the electron-ion complex and the spin-orbit interaction which results in a breakdown of LS coupling. Effects of spin-orbit interaction alone on photoelectron angular distributions have been theoretically analyzed recently by Walker and Waber [T. E. H. Walker and J. T. Waber, Phys. Rev. Letters 30, 307 (1973)]. As these authors point out, their results are an example of the angular-momentum-transfer formulation and, in fact, can be obtained directly from the general expression for the angular distribution given below [Eq. (8)]. Nonetheless, it is important to realize that spin-orbit interactions are but one mechanism for the production of multiple angular momentum transfers.

II. ANGULAR-MOMENTUM-TRANSFER FORMULATION OF ANGULAR CORRELATIONS

The differential cross section for the ionization (1) is given by

$$\frac{d\sigma}{d\Omega}=\frac{\sigma}{4\pi}\left[1+\beta P_2(\cos\theta)\right], \quad (5)$$

where σ is the integrated cross section and the asymmetry parameter β pertains to light linearly polarized along the z axis. The resolution of the differential cross section into components with dif-

ferent angular momentum transfers proceeds as follows[2]: The allowed j_t values are determined from Eqs. (2)–(4). Then one determines an asymmetry parameter β for each value of j_t according to whether the parity change in the target is $\pm(-1)^{j_t}$: Values of j_t for which $\pi_0\pi_c=(-1)^{j_t}$ are said to be parity favored and have an asymmetry parameter

$$\beta(j_t)_{\text{fav}}=\frac{(j_t+2)|\bar{S}_+(j_t)|^2+(j_t-1)|\bar{S}_-(j_t)|^2-3[j_t(j_t+1)]^{1/2}[\bar{S}_+(j_t)\bar{S}_-(j_t)^\dagger+\bar{S}_+(j_t)^\dagger S_-(j_t)]}{(2j_t+1)[|\bar{S}_+(j_t)|^2+|\bar{S}_-(j_t)|^2]}\ , \tag{6}$$

where $S_\pm(j_t)$ denotes the photoionization amplitude[6] for a given j_t and for $l=j_t\pm1$; values of j_t for which $\pi_0\pi_c=-(-1)^{j_t}$ are called parity unfavored and have a $\sin^2\theta$ angular distribution, i.e.,

$$\beta(j_t)_{\text{unf}}=-1\ , \tag{7}$$

independently of dynamics. The observed asymmetry parameter is an average over the asymmetry parameters $\beta(j_t)$, weighted by the corresponding partial integrated cross sections $\sigma(j_t)$,

$$\beta=\Big(\sum_{j_t}^{\text{fav}}{}'\,\sigma(j_t)\beta(j_t)-\sum_{j_t}^{\text{unf}}{}'\,\sigma(j_t)\Big)\Big/\sum_{j_t}\sigma(j_t)\ . \tag{8}$$

In (8) the primed sums are over only the parity-favored and parity-unfavored j_t values, respectively. The integrated cross sections have the structure

$$\sigma(j_t)_{\text{fav}}=\pi\lambda\!\!\!^{-2}[(2j_t+1)/(2J_0+1)]\times[|\bar{S}_+(j_t)|^2+|\bar{S}_-(j_t)|^2]\ , \tag{9}$$

$$\sigma(j_t)_{\text{unf}}=\pi\lambda\!\!\!^{-2}[(2j_t+1)/(2J_0+1)]\,|\bar{S}_0(j_t)|^2\ , \tag{10}$$

where $\bar{S}_0(j_t)$ is the photoionization amplitude[6] for the value of j_t equal to the escape orbital momentum l; $\lambda\!\!\!^{-}$ is the photon wavelength (divided by 2π).

The expression (8) for β is the essential tool of our analysis. It is a general result, following only from the specification of the total angular momentum and parity of each element of the ionization reaction.[2] No assumptions are required about angular-momentum coupling schemes or indeed in regard to any details of internal structure of the various reactants (e.g., atom or molecule, charged or neutral). Accordingly, (8) embodies a very general conceptual framework with which to analyze effects of autoionization on photoelectron angular distributions.

That photoelectron angular distributions should vary markedly with energy across a resonance in the integrated cross section σ follows from the analytical structure of this asymmetry parameter β: σ and β are merely two sides of the same coin, namely, alternative manifestations of the resonant behavior of ionization amplitudes that is characteristic of autoionization. That is, a resonance in σ implies and is implied by a resonance in β. Note however that, whereas the integrated cross section depends only on the squared moduli of the ionization amplitudes, the asymmetry parameter depends as well on the moduli and phases of these amplitudes through the interference terms in the $\beta(j_t)_{\text{fav}}$. Therefore, the resonance in β can be an even more pronounced spectral feature than the resonance in σ.

That autoionization may enhance the role of otherwise weak terms of (8) can be seen as follows[3]: The initial stage of photoabsorption imparts $j_\gamma=1$ units of orbital momentum to the photoelectron, which has initially orbital momentum $\vec{l}_0$, yielding an orbital momentum

$$\vec{l}'=\vec{j}_\gamma+\vec{l}_0\ . \tag{11}$$

At this point the angular momentum transfer is

$$\vec{j}_t'=-\vec{l}_0=\vec{j}_\gamma-\vec{l}'\ , \tag{12}$$

with the single value $j_t'=l_0$. Additional angular momentum transfers are in general allowed, arising from anisotropic interactions of the photoelectron with the rest of the target (including its own spin) during its subsequent escape. Such interactions—*both electrostatic (orbit-orbit) and magnetic (spin-orbit)*—can change the orientation and even the magnitude of the orbital momentum from $\vec{l}'$ to $\vec{l}$, thereby resulting in additional angular momentum transfers $\vec{j}_t-\vec{j}_t'$. Of course, the electron must interact with a nonzero angular momentum, for only in that case will it experience a torque and thereby be able to exchange angular momentum. [Thus, e.g., interaction with a $^1S_0$ core, even if polarized, cannot be lead to exchange of angular momentum.] Now autoionization consists of the decay of a bound state in which the electron experiences a protracted and generally anisotropic interaction with the core. This extended interaction should enhance the angular momentum transfers in addition to $j_t'=l_0$. In contrast, the Cooper–Zare model,[1] for example, implies complete absence of any anisotropic electron-core interaction and leads to a formula obtained from (8) by setting $j_t=l_0$ and

$$\bar{S}(l_0)=i^{-l}e^{i\delta_l}(l\,||C^{[1]}||\,l_0)R(l,l_0)\ , \tag{13}$$

where R is a reduced radial dipole matrix element and the other symbols have their usual meaning.[2,3]

Therefore, the measurement of resonances in photoelectron angular distributions should yield results that can deviate considerably from those predicted by the Cooper–Zare model.

III. EXAMPLES

We have then pointed out two key elements of the effect of autoionization on photoelectron angular distributions: One is the sharp spectral variation of β and the other is the enhanced importance of alternative angular momentum transfers. To illustrate these resonant features of photoelectron angular distributions we shall consider examples from the photoionization of xenon and mercury.

A. Autoionization in Xenon

Ionization of xenon leaves the ion in a doublet ground state,

$$\mathrm{Xe}(5p^6\ {}^1S_0)+\gamma(j_\gamma=1,\ \pi_\gamma=-1) \rightarrow \mathrm{Xe}^+(5p^5\ {}^2P^\circ_{3/2,1/2})+e(l=0,\ 2)\ . \quad (14)$$

The ionization potential for production of the lower level $^2P^\circ_{3/2}$ of the ion doublet is $I_{3/2}=12.127$ eV, and the doublet splitting is $I_{1/2}-I_{3/2}=1.43$ eV. The spectral region between these fine-structure thresholds was found by Beutler[7] long ago to consist of a Rydberg series of autoionization resonances, with widths comparable to their level separations. The autoionization consists of the escape of an electron, initially bound to the $^2P^\circ_{3/2}$ core. It is represented schematically by

$$\left.\begin{matrix}5p^5(^2P^\circ_{1/2})nd\\ 5p^5(^2P^\circ_{1/2})n's\end{matrix}\right\} \xrightarrow[J=1,\ \pi=-1]{\text{autoionization}} \left\{\begin{matrix}5p^5(^2P^\circ_{3/2})\epsilon d\\ 5p^5(^2P^\circ_{3/2})\epsilon s\end{matrix}\right. .$$

Only the total angular momentum ($J=1$) and parity ($\pi=-1$) are necessarily conserved in the autoionization. In particular, the orbital momentum $\vec{l}$ of the photoelectron can be changed by the autoionization process.

The Rydberg character of the series of autoionizing levels emerges when this spectral region is mapped onto the scale of the effective quantum number $\nu_{1/2}$ with respect to the upper threshold $I_{1/2}$ of the ion doublet. This quantum number is defined by

$$\hbar\omega = I_{1/2} - 1/2\nu^2_{1/2}\,, \quad (15)$$

where energies are in atomic units. The mapping reveals that each pair of Rydberg levels, $5p^5(^2P^\circ_{1/2})nd$ and $5p^5(^2P^\circ_{1/2})n's$, fits within one unit of $\nu_{1/2}$, and that the Beutler–Fano resonance profiles repeat unchanged with period one in $\nu_{1/2}$. On the other hand, owing to the nonlinear relationship between the energy $\hbar\omega$ and the effective quantum number $\nu_{1/2}$, the profile widths and separations decrease rapidly on the energy scale from about 0.44 eV ($3.5 \leq \nu_{1/2} \leq 4.5$) just above the $^2P^\circ_{3/2}$ threshold to zero ($\nu_{1/2}=\infty$) at the $^2P^\circ_{1/2}$ threshold.

The linearity and periodicity of the Rydberg series on the $\nu_{1/2}$ scale is a central element of the theoretical understanding of these resonances, i.e., the whole autoionization region can be understood from the properties of the spectrum over a single unit range of $\nu_{1/2}$. Here, then, we want to determine the angular distribution of photoelectrons ejected into this spectral region and we will do this for the single unit range $3.5 \leq \nu_{1/2} \leq 4.5$.

The first step is to analyze the ionization process (14) according to the scheme outlined in Sec. II. The angular momentum and parity quantum numbers are

$$\begin{aligned} &J_0=0\,, \quad j_\gamma=1\,, \quad J_c=\tfrac{3}{2}\,, \quad l=0,\ 2,\\ &\pi_0=+1\,, \quad \pi_\gamma=-1\,, \quad \pi_c=-1\,, \quad \pi_l=+1\,. \end{aligned} \quad (16)$$

Note that $J_c=\frac{3}{2}$ since we consider only photon energies below $I_{1/2}$; $\pi_l=+1$ is determined by parity balance with $\pi=-1$; $l=0,\ 2$ is then fixed by angular momentum balance with $J=1$. The angular momentum transfers allowed are then determined by Eq. (2) to be

$$\begin{aligned} &j_t=1 \text{ (parity favored)} \quad \text{for } l=0,\ 2,\\ &j_t=2 \text{ (parity unfavored)} \quad \text{for } l=2\ . \end{aligned} \quad (17)$$

Note that odd j_t values are parity favored since $\pi_0\pi_c=-1$, and that s waves ($l=0$) contribute only to the parity-favored component. For this case, the asymmetry parameter (8) is then

$$\beta=[\sigma(1)\beta(1)-\sigma(2)]/[\sigma(1)+\sigma(2)]\,. \quad (18)$$

Now from (6) we have

$$\beta(1)=\frac{3|\bar{S}_d(1)|^2-3(2)^{1/2}\,[\bar{S}_d(1)\bar{S}_s(1)^\dagger+\bar{S}_d(1)^\dagger\bar{S}_s(1)]}{3[\,|\bar{S}_d(1)|^2+|\bar{S}_s(1)|^2\,]}\,, \quad (19)$$

and (9) and (10) give

$$\sigma(1)=3\pi\lambda^2[\,|\bar{S}_d(1)|^2+|\bar{S}_s(1)|^2\,], \quad (20)$$

$$\sigma(2)=5\pi\lambda^2|\bar{S}_d(2)|^2\,, \quad (21)$$

where the subscripts $+$, $-$, 0, on $\bar{S}(j_t)$ are replaced with s or d for $l=0$ or $l=2$. Therefore the asymmetry parameter is given by

$$\beta=\frac{|\bar{S}_d(1)|^2-\frac{5}{3}\,|\bar{S}_d(2)|^2-\sqrt{2}\,[\bar{S}_d(1)\bar{S}_s(1)^\dagger+\bar{S}_d(1)^\dagger\bar{S}_d(1)]}{|\bar{S}_d(1)|^2+\frac{5}{3}\,|\bar{S}_d(2)|^2+|\bar{S}_s(1)|^2}\,. \quad (22)$$

The parity-unfavored contribution to the asymmetry parameter (22) is given by the photoelectric intensity $|S_d(2)|^2$ for ejection of d waves into the continuum with the transfer of two units of angular momentum. The physical origin here of $j_t=2$ is the spin-orbit final-state interaction which causes a breakdown of LS coupling as the electron escapes

from the ion core. This may be seen by expressing Eq. (2) for $\vec{j}_t$ in terms of the approximately good LS quantum numbers of the ion core, i.e.,

$$\vec{j}_t = \vec{L}_c + \vec{S}_c + \vec{s}\,, \tag{23}$$

using the fact that $J_0 = 0$. Now the electrons are originally coupled into a singlet; i.e., before photoabsorption the photoelectron's spin was *antiparallel* to the net spin of the rest of the atom. In the absence of spin-orbit interaction in the final state the spins would remain antiparallel and therefore yield $\vec{S}_c + \vec{s} = 0$ in (23). Thereby j_t would be limited to the single value $j_t = L_c = 1$. Therefore, the contribution of the $j_t = 2$ component to (22) is an index of the effects of spin-orbit interaction on the photoionization process.

To determine the angular distribution quantitatively, the transition amplitudes $\bar{S}_l(j_t)$ must be evaluated. This is done in two steps. First the $\bar{S}_l(j_t)$ are expressed in terms of the more familiar reduced dipole transition amplitudes $P_l^{[1]}(J)$ characterized by the total angular momentum J. Then, the matrix elements $P_l^{[1]}(J)$ are determined semiempirically using the multichannel quantum-defect theory (MQDT).[8] The $P_l^{[1]}(J)$ are evaluated in terms of the interaction parameters of the MQDT, which have been determined[8(d)] by fitting theory to spectroscopic measurements.

Reduced Dipole Matrix Elements $P_l^{[1]}(J)$

The formulation of DF, summarized in Sec. II, expresses angular distribution in terms of rotationally invariant matrix elements of a scattering operator S, which connects the initial state (target + photon) to the final state (residual ion + electron) and which is characterized by the angular momentum transferred between unobserved elements of the "scattering process." These matrix elements are written

$$\bar{S}_l(j_t) \equiv ((J_c s)J_{cs} l \,|\, \bar{S}(j_t) \,|\, J_0 j_\gamma = 1)\,. \tag{24}$$

The formulation in terms of S matrix elements derives from the original treatment[9] which is designed for a class of reactions more general than photoprocesses. The formulation in terms of j_t exploits the incoherence of the angular momentum transferred between unobserved reactants to represent the differential cross section by separate characteristic contributions for the various j_t. On the other hand, photoionization *calculations* are conveniently done in terms of the more familiar reduced dipole matrix elements, rather than S matrix elements, characterized by the total angular momentum J of the process, rather than the angular momentum transfer j_t. Two steps are required to establish the connection between the amplitudes $\bar{S}_l(j_t)$ and the reduced dipole transition amplitudes. First, the connection is given between the scattering amplitudes $\bar{S}_l(j_t)$ and S matrix elements[9]

$$S_l(J) \equiv ((J_c s)J_{cs} l \,|\, S(J) \,|\, J_0 j_\gamma = 1)\,, \tag{25}$$

characterized by the total angular momentum J of the whole system. Then the scattering amplitudes $S_l(J)$ are expressed in terms of the usual reduced dipole matrix elements[10]

$$P_l^{[1]} \equiv ((J_c s)J_{cs} l,\, J- \,||P^{[1]}||\, J_0)\,, \tag{26}$$

normalized with the incoming-wave boundary conditions (denoted by the minus sign) that are appropriate to photoionization.

The amplitudes $\bar{S}_l(j_t)$ and $S_l(J)$ are shown in Ref. 9 to be related by the recoupling expansion

$$((J_c s)J_{cs} l \,|\, \bar{S}(j_t) \,|\, J_0 j_\gamma = 1) = \sum_J (-1)^{J_0 - J - 1}(2J+1) \times \begin{Bmatrix} l & J_{cs} & J \\ J_0 & 1 & j_t \end{Bmatrix} ((J_c s)J_{cs} l \,|\, S(J) \,|\, J_0 j_\gamma = 1)\,. \tag{27}$$

The connection between the amplitudes $S_l(J)$ and $P_l^{[1]}(J)$ is found by comparing the alternative expressions[11] for the photoionization cross section given in terms of these amplitudes by

$$\sigma = 4\pi^2 \alpha \hbar\omega (2J_0+1)^{-1} \times \sum_{M_c \mu m M_0} \sum_l |(J_c M_c, s\mu, lm, - |P_{m_\gamma}^{[1]}| J_0 M_0)|^2\,, \tag{28a}$$

$$\sigma = 3\pi\lambda\!\!\!^{-2}(2J_0+1)^{-1} \times \sum_{M_c \mu m M_0} \sum_l |(J_c M_c, s\mu, lm|S|J_0 M_0, j_\gamma m_\gamma)|^2\,. \tag{28b}$$

In (28) the summations over m quantum numbers and the factor $(2J_0+1)^{-1}$ arise from averaging over the initial magnetic substates and summing over the final magnetic substates and spin polarizations. Using the expansions[12]

$$(J_c M_c, s\mu, lm, - |P_{m_\gamma}^{[1]}| J_0 M_0) = \sum_{J_{cs} J} (2J+1)^{-1/2}(J_c M_c, s\mu, lm \,|\, (J_c s)J_{cs} l, JM) \times ((J_c s)J_{cs} l,\, J- \,||P^{[1]}||\, J_0)(JM \,|\, J_0 M_0, j_\gamma m_\gamma)\,, \tag{29a}$$

$$(J_c M_c, s\mu, lm|S(J)|J_0 M_0, j_\gamma m_\gamma) = \sum_{J_{cs} J} (J_c M_c, s\mu, lm \,|\, (J_c s)J_{cs} l, JM) \times ((J_c s)J_{cs} l \,|\, S(J) \,|\, J_0 j_\gamma)(JM \,|\, J_0 M_0, j_\gamma m_\gamma)\,, \tag{29b}$$

and the symmetry and orthonormality of the Wigner coefficients,[13] the summations over m quantum numbers can be carried out to give

$$\sigma = \tfrac{4}{3}\pi^2 \alpha \hbar\omega (2J_0+1)^{-1} \times \sum_{J_{cs} J l} |((J_c s)J_{cs} l,\, J- \,||P^{[1]}||\, J_0)|^2\,, \tag{30a}$$

$$\sigma = \pi\lambda\!\!\!^{-2}(2J_0+1)^{-1}$$

$$\times \sum_{J_{cs}J'} (2J+1)\left|((J_cS)J_{cs}l\left|S(J)\right|J_0 j_\gamma=1)\right|^2 . \quad (30b)$$

Comparison of the two expressions (30) gives the desired connection,

$$((J_cS)J_{cs}l\left|S(J)\right|J_0 j_\gamma=1) = n(\lambda)(2J+1)^{-1/2}((J_cS)J_{cs}l, J-\left|\left|P^{[1]}\right|\right|J_c), \quad (31)$$

$$n(\lambda)^2 = 4\pi^2\alpha\hbar\omega/3\pi\lambda^2 . \quad (32)$$

For the xenon example we have $J_0=0$, and therefore J is restricted to the single value $J=j_\gamma=1$ and $J_{cs}=j_t$. Accordingly, substitution of (31) into (27) gives

$$((J_cS)J_{cs}=j_t l\left|\bar{S}(j_t)\right|J_0=0,\ j_\gamma=1) = n(\lambda)(2j_t+1)^{-1/2}(-1)^{1+j_t} \times((J_cS)J_{cs}=j_t l,\ J=1-\left|\left|P^{[1]}\right|\right|J_0=0), \quad (33)$$

for the connection between the amplitudes $\bar{S}_l(j_t)$ and $P_l^{[1]}(J=1)$.

Before proceeding to the evaluation of the amplitudes $P_l^{[1]}(J)$, it is important to note one new aspect of the expansions (29), not included in the corresponding expansion equation (5) or Ref. 9. This is the explicit account taken here of the photoelectron spin. This introduces an additional summation over the total *unobserved* final-state angular momentum J_{cs}.[14] With this additional feature, the whole analysis of Ref. 9 carries through as before with the following additional result. The final-state angular momentum J_{cs} is incoherent in both the differential and integrated cross section, just as j_t is incoherent, since the orientation of the core (M_c) and the spin polarization of the photoelectron (μ) are unobserved, and $d\sigma/d\Omega$ must be summed over all possible values of J_{cs} [compare (30)]. This means that the expressions given in Sec. II for σ and $\sigma\beta$ must in general be summed over J_{cs}. Often, however, as for the xenon example and, as we shall see, for the mercury example as well, only a single value of J_{cs} occurs.

Evaluation of $P_l^{[1]}(J)$ by MQDT

A fundamental concept of the MQDT is the resolution of the ionization process into an initial photon absorption and the photoelectron's subsequent interaction with, and escape from, the target. These two aspects of the process contribute different characteristic elements to the ionization dynamics. Photon absorption occurs inside the atom and is characterized by real transition amplitudes

$$D_\alpha = (\alpha J=1\left|\left|P^{[1]}\right|\right|J_0=0) \quad (34)$$

connecting the atomic ground state to close-coupling eigenstates $(\alpha|$ which depend on the electron-core interaction at short range. [These eigenstates $(\alpha|$, with *standing-wave* normalization, are discussed in Ref. 8(c).] Electron escape, on the other hand, probes the effects of long-range interaction, in particular, the temporary retention of the electron by the $^2P^\circ_{1/2}$ ion to form autoionizing states. The electron escape is characterized by the eigenchannels $(\rho|$ of elastic scattering of the electron by the xenon ion in the $^2P^\circ_{3/2}$ level in the range of electron kinetic energies $\epsilon < I_{1/2}-I_{3/2}=1.43$ eV, with the whole system having angular momentum $J=1$ and odd parity. Retention of the electron in an autoionizing state through excitation of the ion from the $^2P^\circ_{3/2}$ level to the $^2P^\circ_{1/2}$ level, causes the elastic scattering phase shifts $\pi\tau_\rho$ to experience a pronounced spectral variation that is the earmark of multichannel resonance. This energy dependence is described below and discussed in detail in Ref. 8(c). It constitutes a central aspect of the MQDT treatment [see especially Fig. 2 of Ref. 8(c)]. In essence, the sum of the phase shifts $\pi\tau_\rho$ for all channels $(\rho|$ undergoes a net increase of 2π for every unit range of $\nu_{1/2}$, i.e., every time the energy passes through the combined Beutler–Fano profile of the two $(ns, n'd)\rightarrow(\epsilon s, \epsilon d)$ autoionization resonances.

The dipole matrix elements $P_l^{[1]}$ are expressed in terms of the amplitudes D_α in two steps. First, the final states $((J_cS)J_{cs}l, J|$, with *standing-wave* normalization (i.e., without the "minus" quantum number) are expanded into the elastic-scattering channels $(\rho|$ and then re-expanded in terms of the close-coupling eigenchannels $(\alpha|$. This represents *real* dipole transition amplitudes as

$$((J_cS)J_{cs}l, J=1\left|\left|P^{[1]}\right|\right|J_0=0) = \sum_{\rho\alpha}((J_cS)J_{cs}l\left|\rho\right)(\rho\left|\alpha\right)D_\alpha , \quad (35)$$

in terms of *real* transformation coefficients $(J_{cs}l|\rho)$ and $(\rho|\alpha)$. Next, the change is made from standing-wave to incoming-wave normalization through multiplication by the phase factor

$$\exp[i(\sigma_{lJ_c}-\tfrac{1}{2}l\pi+\pi\tau_\rho)] = i^{-l}\exp[i(\sigma_{lJ_c}+\pi\tau_\rho)] . \quad (36)$$

In (36) σ_{lJ_c} is the Coulomb phase $\arg\Gamma(l+1-i/k)$, which is determined by the electronic orbital momentum l and kinetic energy $\epsilon(\text{a.u.})=\frac{1}{2}k^2$ in the $J_c=\frac{3}{2}$ channel. The result is then

$$((J_cS)J_{cs}l, J=1-\left|\left|P^{[1]}\right|\right|J_0=0) = i^{-l}e^{i\sigma_{lJ_c}}\sum_{\rho\alpha}((J_cS)J_{cs}l\left|\rho\right)e^{i\pi\tau_\rho}(\rho\left|\alpha\right)D_\alpha . \quad (37)$$

In the Appendix it is shown how the various elements of this expansion—the transition amplitudes D_α, the transformation matrices $(\rho|\alpha)$ and $(J_{cs}l|\rho)$, and the phase shifts $\pi\tau_\rho$—are determined in terms of the interaction parameters of the MQDT. These interaction parameters in turn have been determined for our purposes by C. M. Lee[8(d)] and are tabulated in the Appendix. Also, in the Appendix a simple

method is given for the evaluation of the Coulomb phase shift differences $\sigma_{j_t+1} - \sigma_{j_t-1}$ which occur in the interference term of $\beta(j_t)_{\text{tav}}$.

The spectral variation of the phase shifts $\pi\tau_\rho$ determine the resonance pattern of both the integrated cross section σ and the asymmetry parameter β. As outlined in the Appendix, in addition to the explicit dependence on τ_ρ in (37), both sets of transformation coefficients, $(J_{cs} l | \rho)$ and $(\rho | \alpha)$, depend on the τ_ρ through functions $\sin\pi\tau_\rho$ or $\cos\pi\tau_\rho$. The dipole transition amplitude (37) contains the additional multiplicative factor $e^{i\pi\tau_\rho}$, and is therefore invariant to the transformation $\tau_\rho \rightarrow \tau_\rho + 1$. Now each τ_ρ is a strongly nonlinear but monotonically increasing function of $\nu_{1/2}$. This functional dependence is characteristic for each ρ. Under the transformation $\nu_{1/2} \rightarrow \nu_{1/2} + 1$, the curves $\tau_\rho(\nu_{1/2})$ for different ρ permute among themselves such that the same set of curves occurs for each unit range of $\nu_{1/2}$. Two of the τ_ρ curves will be shifted upward by 1 in the permutation, corresponding to the net increase by 2π in the elastic-scattering phase shift. But each shift by 1 leaves (37) invariant. Further, since (37) is summed over all ρ, the permutation merely amounts to interchanging terms of the sum, and therefore the permutation also leaves (37) invariant. We therefore obtain the fundamental result that the dipole transition amplitude (37) is invariant under the transformation $\nu_{1/2} \rightarrow \nu_{1/2} + 1$, except for the slight energy dependence of the Coulomb phase.

This invariance accounts for the periodicity of the Rydberg series of autoionizing levels. The periodicity is exact in the integrated cross section, for which the Coulomb phase effect vanishes altogether because of the incoherence of the transition amplitudes for alternative orbital momenta l. Further, the Coulomb phase effect is small in the asymmetry parameter for low $\nu_{1/2}$ and becomes rapidly negligible as $\nu_{1/2}$ increases, owing to the corresponding rapid decrease in the change of electronic kinetic energy per unit range of $\nu_{1/2}$. That is, the resonance profiles in β are themselves very nearly also periodic in $\nu_{1/2}$, with period 1.

The amplitudes for transitions into the channels $(\rho|$ superpose coherently in the angular distribution, and the resulting interference terms are proportional to $\cos(\sigma_d - \sigma_s + \pi\tau_\rho - \pi\tau_{\rho'})$. These interference terms vanish in the integrated cross section (see Appendix) but they cause the angular distribution to contain information not present in the integrated cross section. This circumstance is especially important to the theory for the following reason: The semiempirical fitting procedures used by Lee[8(d)] and earlier by Lu,[8(c)] based on photoabsorption (integrated cross section) measurements, have encountered difficulties which have prevented, so far, the unambiguous determination of all of the interaction parameters of the theory. Independent information contained in measured angular distributions should help in removing these ambiguities. Conversely, however, it should be kept in mind that the measured spectral variation of β may differ from the results given here, owing to these uncertainties in the values of the semiempirical interaction parameters utilized in this paper. Nonetheless, these differences should be minor. The gross features of the β resonance will remain.

Results for Xenon

The results are given graphically in Fig. 1 for one unit range of $\nu_{1/2}$ from $\nu_{1/2} = 3.5$ to $\nu_{1/2} = 4.5$, corresponding to the range of photoelectron kinetic energies $0.196 \leq \epsilon \leq 0.635$ eV. Figure 1(a) gives the integrated cross section σ. The broad maximum peaking at $\nu_{1/2} \approx 0.75$ (modulo 1) is due primarily to autoionization of $5d^5(^2P^\circ_{1/2})nd$. The autoionization of $5d^5(^2P^\circ_{1/2})ns$ is concentrated at the "s resonance" on the high-energy shoulder of the broad peak at $\nu_{1/2} \approx 0.975$. As an index of the strength of parity-unfavored ionization, the ratio

$$r = \sigma(1)/[\sigma(1) + \sigma(2)] \tag{38}$$

is plotted in Fig. 1(b). This ratio could range between 1 for fully parity-favored ($j_t = 1$) ionization, and zero for fully unfavored ($j_t = 2$) ionization. Since s waves contribute only to $\sigma(1)$, r is also an index of the relative strength of s- and d-wave ionization. Finally, in Fig. 1(c) the spectral variation of the asymmetry parameter β is plotted, showing a pronounced resonant structure in the photoelectron angular distribution.

The spectral variation of β shows two striking features as $\nu_{1/2}$ increases: There is first a broad dip (width ≈ 0.1 eV) toward $\beta = -1$ ($j_t = 2$), and then a rapid oscillation (width ≈ 0.06 eV) across the s resonance in the integrated cross section. This behavior can be understood qualitatively when viewed with the corresponding spectral features of σ and r. The broad minimum in β at $\nu_{1/2} \approx 0.64$ occurs when the photoelectric current is a minimum. Further, s-wave ionization is negligible in this region, and the minimum of β is paralleled by a corresponding minimum of r. Then, as the photoelectric current rises and passes through the broad d-resonance maximum in σ, parity-favored d-wave ionization increases, resulting in an increase of r and a corresponding increase of β away from -1. In the region of the s resonance the coupling between the s- and d-wave ionization channels produces sharp variations in the relative contributions of s- and d-wave ionization. These variations are reflected in the rapid oscillation of β across the s resonance: First, immediately below the s resonance, s-wave ionization is depressed and d-wave ionization is enhanced, resulting in a sharp rise of

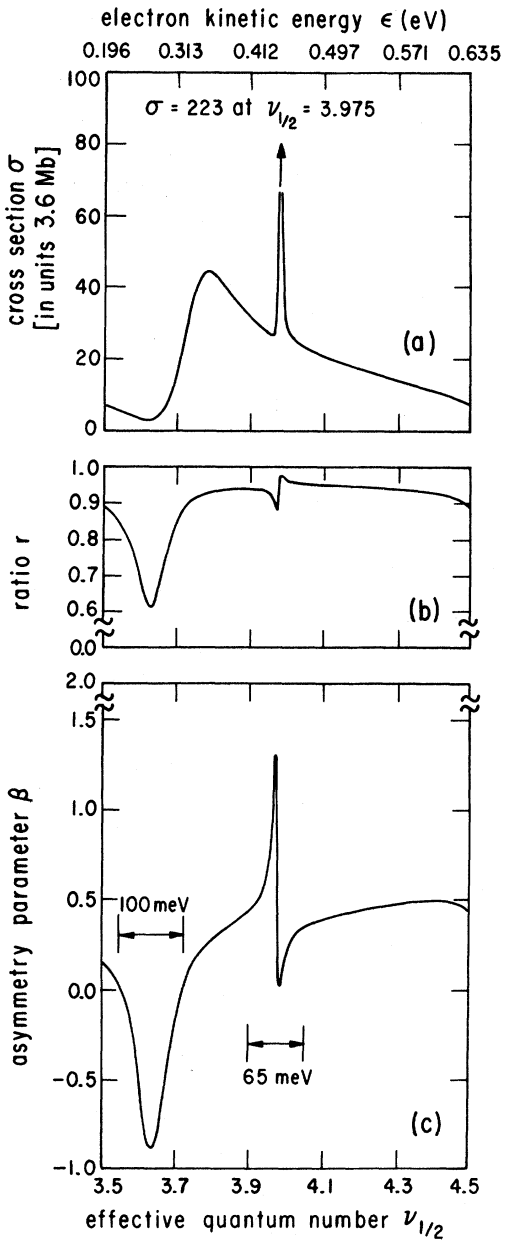

FIG. 1. Plot of xenon autoionization cross section and photoelectron asymmetry parameter resonance for one unit range of $\nu_{1/2}$. (a) Integrated cross section $\sigma=\sigma(1)+\sigma(2)$; (b) dimensionless cross-section ratio $\sigma(1)/\sigma$; (c) asymmetry parameter β. Note the breaks in the ordinate scales, and the nonlinear scale of electron kinetic energies

β away from the s-wave value $\beta=0$, and a corresponding dip of r. Then, s-wave ionization rapidly increases to a peak at the s-resonance maximum, sending β near 0 and r toward 1. Finally, on the high-energy side, s-wave ionization drops off once again, r drops and levels off, and β rises to a smooth plateau.

This cycle will repeat periodically in $\nu_{1/2}$, with period 1, up to the threshold of the $^2P^\circ_{1/2}$ level. The Coulomb phase interference term causes $\beta(\nu_{1/2}=3.5)$ to differ from $\beta(\nu_{1/2}=4.5)$ by 0.3.

An analogous β resonance occurs in all of the rare gases, and in fact the calculations also have been performed for argon, showing results similar to those for xenon. The xenon example is given here since xenon has the broadest resonances and therefore is a good candidate for experimental verification.

As pointed out in Sec. II, resonances in β are to be expected, in general, whenever autoionization occurs. Indeed, going to higher photon energies the rare gases provide another example of this effect, in the region of $nsnp^6(^2S_{1/2})n'p \rightarrow ns^2np^5(^2P^\circ) \times[\epsilon s, \epsilon d]$ resonances of the Rydberg series converging to the $nsnp^6\,^2S_{1/2}$ level of the rare-gas ion. These resonances have not been sufficiently well resolved by photoelectron spectroscopy to map the resonant structure of β, but evidence of the effect is already apparent in the measurements by Codling and Mitchell[15] for argon and in the recent results of Van der Wiel and Brion[16] on neon.

B. Autoionization in Mercury

As a further example consider the photoionization of mercury below the first excited state of the mercury ion. Production of the ion ground state,

$$\mathrm{Hg}(5d^{10}6s^2\ ^1S_0)+\gamma(j_\gamma=1,\ \pi_\gamma=-1) \rightarrow \mathrm{Hg}^+(5d^{10}6s\ ^2S_{1/2})+e(l=1), \qquad (39)$$

has an ionization potential of 10.43 eV. Embedded in this ionization continuum are autoionizing Rydberg levels $5d^96s^2(^2D)np$ and $5d^96s^2(^2D)n'f$ converging to the first excited term $5d^96s^2(^2D)$ of the ion.[17] The lower level $^2D_{5/2}$ of the doublet has the ionization potential 14.83 eV, and the spin-orbit interaction raises the $^2D_{3/2}$ level 1.87 eV higher. Autoionization occurs between these fine structure ^2D thresholds, analogous to the xenon example, but here we consider rather autoionizing levels in the 4.43-eV spectral range between the $^2S_{1/2}$ and $^2D_{5/2}$ levels of different terms.

This first autoionization region provides a striking example of the theory. Owing to parity and angular momentum conservation, the electron must leave the atom with the single orbital momentum $l=1$. The Cooper–Zare formula[1] then predicts that the electron is ejected with full anisotropy, i.e., that the angular distribution is fixed at $\cos^2\theta$ ($\beta=2$), independently of dynamics, throughout the whole spectral range. Actually, this will be the case only if the spin of the photoelectron and the net spin of the rest of the atom *remain coupled into a singlet through the ionization process*, for only then must the electron necessarily carry away the full anisotropy of the photon-atom interaction. If ionization

proceeds through autoionizing levels in which the spins are coupled into a triplet, then the angular distribution can be *depolarized by the unobserved nonzero spin*[18] and β can deviate from 2.

The angular-momentum-transfer analysis of the ionization reaction provides the quantitative basis for these ideas. Since $J_0 = 0$ and $J_c = S_c = \frac{1}{2}$, the angular momentum transfer (2) becomes for this case

$$\vec{j}_t = \vec{S}_c + \vec{s} . \tag{40}$$

Thus the allowed angular momentum transfers are

$$\begin{aligned} &j_t = 0 \quad \text{(parity favored,} \quad \beta = 2), \\ &j_t = 1 \quad \text{(parity unfavored,} \quad \beta = -1). \end{aligned} \tag{41}$$

If the spins remain antiparallel, then only $j_t = 0$ can occur and from (6), $\beta = 2$ as predicted by the Cooper–Zare formula. On the other hand, $j_t = 1$, with $\beta = -1$, arises because spin-orbit forces disturb this singlet coupling. The observed asymmetry parameter is [cf. (6) and (8)]

$$\beta = [2\sigma(0) - \sigma(1)]/[\sigma(0) + \sigma(1)], \tag{42}$$

which ranges from $\beta = 2$ ($\cos^2\theta$) for fully-parity-favored ionization, to $\beta = -1$ ($\sin^2\theta$) for fully-parity-unfavored ionization. From (9) and (10) the integrated cross sections are given by

$$\begin{aligned} \sigma(0) &= \pi\lambda^2 |\bar{S}_p(0)|^2 , \\ \sigma(1) &= 3\pi\lambda^2 |\bar{S}_p(1)|^2 . \end{aligned} \tag{43}$$

However, from (33), the matrix elements $\bar{S}_p$ are directly proportional to the corresponding reduced dipole matrix elements $P_p^{[1]}$, and the angular distribution depends only on the ratio of p-wave ionization with $j_t = 0$ or $j_t = 1$. This dependence is conveniently characterized by a strength parameter

$$s = \frac{|P_p^{[1]}(0)|^2 - |P_p^{[1]}(1)|^2}{|P_p^{[1]}(0)|^2 + |P_p^{[1]}(1)|^2} , \tag{44}$$

which ranges from $s = 1$ for fully-parity-favored ionization, through $s = 0$ for equal intensity with $j_t = 0$ and $j_t = 1$, to $s = -1$ for fully-parity-unfavored ionization. In terms of s the asymmetry parameter (42) becomes

$$\beta = \tfrac{1}{2}(3s + 1) , \tag{45}$$

i.e., $\beta = 2$ for $s = 1$, $\beta = \frac{1}{2}$ for $s = 0$, and $\beta = -1$ for $s = -1$.

Niehaus and Ruf[5] have measured β at two closely spaced energies in the $^2S_{1/2} - {}^2D_{5/2}$ spectral region, using the ArI doublet resonance lines at 11.63 and 11.83 eV. The lower line falls on the high-energy shoulder of the autoionizing level $[5d^9(^2D_{3/2})6s^2] \times 6p_{3/2}\,{}^3D_1^\circ$ for which the electron and core spins are coupled into a *triplet*.[19] At this lower energy they find $\beta = 1.25 \pm 0.1$, corresponding to $s = 0.5$. At 11.83 eV they find $\beta = 2.13 \pm 0.1$, corresponding to $s = 1.0$. [For dipole ionization β can be no larger than 2 and therefore this latter value may reflect experimental uncertainty.] Over an energy range of 0.2 eV the strength parameter changes by a factor of 2. This indicates that indeed parity-unfavored ionization is substantial in this autoionization spectral region. It would be very desirable to fully map the spectral variation of β throughout this range.

IV. CONCLUSION

Resonant structure in photoelectron angular distributions is predicted to be a general feature of all atomic and molecular autoionization resonances. These β resonances are sensitive probes of atomic and molecular dynamics. They can determine the cumulative effects of forces that might go undetected in direct ionization. Owing to the interferences present in all angular distribution measurements, the measured β spectra contain new and independent dynamical information not available in integrated cross sections. The experimental investigation of these angular distribution resonances is an essentially untapped and rich resource of information for chemical physics.

ACKNOWLEDGMENT

I am grateful to Professor U. Fano for valuable discussions and for his encouragement.

APPENDIX

MQDT Interaction Parameters

The reduced dipole matrix elements (37) are evaluated for xenon in terms of the following interaction parameters, which have been obtained by Lee.[8(d)] (i) One set of parameters consists of five real dipole transition amplitudes D_α. The quantum number α of the close-coupling eigenchannels runs from 1 to 5 and corresponds approximately to the five LS channels of the electron–ion-core system at short range, with $J = 1$ and $\pi = -1$:

$$\begin{aligned} &\alpha = \quad 1 \quad , \quad 2 \quad , \quad 3 \quad , \quad 4 \quad , \quad 5 \quad ; \\ &LS \text{ channel} = p^5d\ {}^3D_1^\circ,\ p^5d\ {}^1P_1^\circ,\ p^5d\ {}^3P_1^\circ,\ p^5s\ {}^3P_1^\circ,\ p^5s\ {}^1P_1^\circ . \end{aligned} \tag{A1}$$

The values of D_α, normalized per unit energy range in atomic units, are

$$\alpha = \quad 1 \quad , \quad 2 \quad , \quad 3 \quad , \quad 4 \quad , \quad 5 \quad ;$$
$$D_\alpha/\sqrt{3} = -0.28462 \, , \; 4.09991 \, , \; -0.50779 \, , \; -0.03106 \, , \; 1.83506 \, . \tag{A2}$$

The factor $1/\sqrt{3}$ in (A2) is necessary because the D_α, as defined here by Eq. (34), are rotationally invariant matrix elements of r, whereas Lee[8(d)] and Lu[8(c)] define the D_α as matrix elements of z [see Eq. (2.4) of Ref. 8(c)]. The two definitions are made equivalent through multiplication by $\langle (z/r)^2 \rangle^{1/2} = 1/\sqrt{3}$. With this normalization, the unit of cross section $\pi\lambda\!\!\!^{-2} n (\lambda\!\!\!^{-})^2$ [see Eqs. (20), (21), (32), and (33)] is determined by setting $\lambda^{-1} = I_{3/2}$, since the MQDT interaction parameters are assumed to be constant throughout the autoionization range from $I_{3/2}$ to $I_{1/2}$.[8(c)] This gives $\pi\lambda\!\!\!^{-2} n (\lambda_{3/2})^2 = 3.6$ Mb.

(ii) Another set of parameters consists of five close-coupling eigenphase shifts $\pi\mu_\alpha$, or the equivalent quantum defects

$$\alpha = \quad 1 \quad , \quad 2 \quad , \quad 3 \quad , \quad 4 \quad , \quad 5 \quad ;$$
$$\mu_\alpha = 0.360 \, , \; 0.120 \, , \; 0.560 \, , \; 0.040 \, , \; -0.007 \, . \tag{A3}$$

(iii) The last set of parameters forms the 5×5 orthogonal transformation matrix

$$U_{i\alpha}^{(J=1)} \equiv (J_c(ls)j \,|\, \alpha)^{(J=1)} \, , \tag{A4}$$

connecting the close-coupling eigenchannels $(\alpha J|$ to the asymptotic jj-coupled dissociation channels $(J_c(ls)j, J|$. In (A4), the quantum number i of the dissociation channels is given by

$$i = \quad 1 \quad , \quad 2 \quad , \quad 3 \quad , \quad 4 \quad , \quad 5 \quad ;$$
$$jj \text{ channel} = {}^2P^\circ_{3/2} d_{5/2} \, , \; {}^2P^\circ_{3/2} d_{3/2} \, , \; {}^2P^\circ_{3/2} s_{1/2} \, , \; {}^2P^\circ_{1/2} d_{3/2} \, , \; {}^2P^\circ_{1/2} s_{1/2} \, . \tag{A5}$$

The transformation matrix is

$$U = \begin{array}{c|ccccc} & \alpha = 1 & 2 & 3 & 4 & 5 \\ i = 4 & 0.67094 & 0.65800 & 0.34073 & -0.00514 & 0.02744 \\ 1 & -0.36223 & 0.69301 & -0.62240 & -0.00545 & -0.03342 \\ 2 & -0.64673 & 0.29448 & 0.70336 & -0.00230 & 0.01741 \\ 5 & 0.01115 & 0.00640 & 0.02454 & 0.81549 & -0.57810 \\ 3 & -0.01573 & 0.00451 & -0.03462 & 0.57871 & 0.81463 \end{array} \, . \tag{A6}$$

and is published here for the first time.[8(d)]

Evaluation of Dipole Transition Amplitudes

Using these interaction parameters, the elements of the expansion (37) are determined as follows: From (A5) we see that there are three elastic-scattering eigenchannels $(\rho|$ open below $I_{1/2}$. The corresponding phase shifts $\pi\tau_\rho$ are determined for each value of $\nu_{1/2}$ as roots of the cubic equation obtained by setting to zero the determinant of the linear system [Sec. III A of Ref. 8(c)]

$$\sum_{j=1}^{3} \Big[-\cot\pi(\nu_{1/2} + \tau_\rho)\delta_{ij} + \Big(\sum_{\alpha=1}^{5} U_{i\alpha} \cot\pi(\nu_{1/2} + \mu_\alpha) U_{\alpha j} \Big) \Big] C_j = 0 \, , \quad i = 1, 2, 3 \, . \tag{A7}$$

The transformation coefficients $(\rho|\alpha)$ which connect the elastic-scattering channels $(\rho|$ to the close-coupling channels $(\alpha|$ is expressed in terms of a vector $\vec{A}$ [defined in Ref. 8(c)] by

$$(\rho \,|\, \alpha) = A_\alpha / N_\rho \, , \tag{A8}$$

where N_ρ is a normalization factor given below. The vector $\vec{A}$ is determined from the system of equations [Eq. (3.23) of Ref. 8(c)]

$$\sum_\alpha U_{i\alpha} \sin\pi(\mu_\alpha - \tau_\rho) A_\alpha = 0 \, , \quad i = 1, 2, 3 \, . \tag{A9}$$

The transformation coefficients $((J_c s) J_{cs} l \,|\, \rho)$ are given by

$$((J_c s) J_{cs} = j_t l \,|\, \rho) = \sum_i ((J_c s) J_{cs} = j_t l \,|\, i = (J_c(ls)j))^{(J=1)} T_{ip} / N_\rho \, , \tag{A10}$$

in terms of the geometrical transformation coefficient

$$((J_c s)J_{cs} = j_t l \,|\, J_c(ls)j)^{(J=1)}$$

$$= (-1)^{J_c+j+1}(2j+1)^{1/2}(2j_t+1)^{1/2}\begin{Bmatrix} \frac{1}{2} & l & j \\ 1 & J_c & j_t \end{Bmatrix}, \quad \text{(A11)}$$

of the dynamical transformation $T_{t\rho}$, given by [see Eq. (3.21) of Ref. 8(c)]

$$T_{t\rho} = \sum_{\alpha} U_{t\alpha} \cos\pi(\mu_\alpha - \tau_\rho) A_\alpha\,, \quad t = 1, 2, 3, \quad \text{(A12)}$$

and of the normalization factor N_ρ, given by

$$N_\rho^2 = \sum_{t=1}^{3} |T_{t\rho}|^2\,. \quad \text{(A13)}$$

Incoherence of Channels ρ in the Integrated Cross Section

The integrated cross section is proportional to

$$\sum_{j_t l} |P_t(j_t)|^2\,. \quad \text{(A14)}$$

But, owing to the orthonormality property

$$\sum_{j_t l} (\rho' \,|\, J_{cs} = j_t l)(J_{cs} = j_t l \,|\, \rho') = \delta_{\rho\rho'}\,, \quad \text{(A15)}$$

(A14) is incoherent in the transition amplitudes for the alternative channels ρ, i.e.,

$$\sum_{j_t l} |P_t(j_t)|^2 = \sum_{\rho=1}^{3}\left(\left|\sum_{\alpha} A_\alpha D_\alpha\right|^2 \Big/ N_\rho^2\right). \quad \text{(A16)}$$

This result corresponds to Eq. (3.25) of Ref. 8(c).

Evaluation of Coulomb Phase Shift Differences

The Coulomb phase difference $\sigma_d - \sigma_s$ which occurs in the interference term of the asymmetry parameter (22) can be conveniently evaluated using the following algebraic scheme which derives from Bethe.[1] The difference $\sigma_{j_t+1} - \sigma_{j_t-1}$ can be represented as the angle of a right triangle whose adjacent side A, opposite side O, and hypotenuse H are given by

$$\begin{aligned} A &= j_t(j_t+1) - (Z/k)^2\,, \\ O &= -(Z/k)(2j_t+1)\,, \\ H &= \{[(j_t+1)^2 + (Z/k)^2][j_t^2 + (Z/k)^2]\}^{1/2}\,, \end{aligned} \quad \text{(A17)}$$

where the ionic charge is Z and the photoelectron kinetic energy is ϵ (a.u.) $= \frac{1}{2}k^2$. These relations are exact and therefore valid for all values of k^2. Thus, e.g., $\cos(\sigma_d - \sigma_s)$ for the xenon example ($Z = 1$) is given by

$$\cos(\sigma_d - \sigma_s) = (2k^2 - 1)/(4k^4 + 5k^2 + 1)^{1/2} \quad \text{(A18)}$$

and is seen to increase monotonically from -1 at $k = 0$ to $+1$ at $k = \infty$. This treatment of Coulomb phase differences is simple and bypasses the numerical errors which may occur when the phase shifts are first calculated separately as arguments of the complex Γ function and then subtracted.

---

*Work supported by U. S. Atomic Energy Commission Contract No. C00-1674-74.

[1] J. Cooper and R. N. Zare, in *Lectures in Theoretical Physics: Atomic Collision Processes*, edited by S. Geltman, K. T. Mahanthappa, and W. E. Brittin (Gordon and Breach, New York, 1969), Vol. XI-C, pp. 317–337; see also H. Bethe, in *Handbuch der Physik*, edited by H. Geiger and K. Scheel (Springer, Berlin, 1933), Vol. 24, Pt. 1, pp. 482–484; P. Auger and F. Perrin, J. Phys. Rad. 8, 93 (1927).

[2] D. Dill and U. Fano, Phys. Rev. Letters 29, 1203 (1972).

[3] D. Dill (unpublished).

[4] D. Dill, Phys. Rev. A 6, 160 (1972).

[5] A. Niehaus and M. W. Ruf, Z. Physik 252, 84 (1972).

[6] A detailed definition of the amplitudes $\overline{S}(j_t)$, in terms of reduced dipole matrix elements, will be given in Sec. III.

[7] H. Beutler, Z. Physik 93, 177 (1935). For recent work see, e.g., K. Yoshino, J. Opt. Soc. Am. 60, 1220 (1970).

[8] The multichannel quantum-defect theory was developed originally by Seaton in (a) M. J. Seaton, Proc. Phys. Soc. (London) A88, 801 (1966). Fano has adapted and extended the theory to the present application in the basic paper (b) U. Fano, Phys. Rev. A 2, 353 (1970), which treats the photoabsorption spectrum of H_2 near threshold. Building on the methods and concepts of Fano's work, Lu developed and applied the MQDT to the semiempirical analysis of the xenon photoabsorption spectrum near the ionization threshold, in (c) K. T. Lu, Phys. Rev. A 4, 579 (1971). C. M. Lee has extended the fitting procedure of Ref. 8(c) in order to obtain the interaction parameters of Lu's analysis in the form required to evaluate the xenon photoelectron angular distribution. This extended fitting procedure will be published shortly, with application to the argon-threshold-region photoabsorption spectrum, in (d) C. M. Lee and K. T. Lu, Phys. Rev. A (to be published); and the xenon parameters are given here in the Appendix. I am indebted to C. M. Lee for providing these results and allowing me to use them prior to publication.

[9] U. Fano and D. Dill, Phys. Rev. A 6, 185 (1972).

[10] See, e.g., B. W. Shore and D. H. Menzel, *Principles of Atomic Spectra* (Wiley, New York, 1968), p. 442, Eq. (8.5).

[11] For the dipole expression in Eq. (28) see, e.g., H. A. Bethe and E. E. Salpeter, *Quantum Mechanics of One- and Two-Electron Atoms* (Springer-Verlag, Berlin, 1957), Eqs. (59.5) and (69.5); for the S-matrix expression see Ref. 8 of U. Fano and D. Dill, Phys. Rev. A 6, 185 (1972), and F. J. Blatt and V. Weisskopf, *Theoretical Nuclear Physics* (Wiley, New York, 1952), pp. 517–521.

[12] The factor $(2J+1)^{-1/2}$ in (29a) arises through application of the Wigner–Eckart theorem.

[13] The properties are the symmetry relation

$$|(JM \,|\, J_0 M_0, j_\gamma m_\gamma)|^2 = \frac{2J+1}{2j_\gamma+1} |(j_\gamma m_\gamma \,|\, JM, J_0 - M_0)|^2,$$

and the orthonormality equations

$$\sum_{M_0} |(j_\gamma m_\gamma \,|\, JM, J_0 - M_0)|^2 = 1,$$

$$\sum_{M_c \mu m} (J_{cs} l J M \mid J_c M_c, s\mu, lm) \times (J_c M_c, s\mu, lm \mid J'_{cs} l J' M) = \delta_{J_{cs} J'_{cs}} \delta_{JJ'}.$$

[14]In this regard see the first two paragraphs of Ref. 9, Sec. I.

[15]P. M. Mitchell and K. Codling, Phys. Letters 38A, 31 (1972).

[16]M. J. Van der Wiel and C. E. Brion, J. Electr. Spectrosc. 1, 739 (1973).

[17]The photoionization spectrum of Hg below the Hg^+ ($^2D_{5/2}$) threshold has been studied by several authors: (a) B. Brehm, Z. Naturforsch. 21a, 196 (1966); (b) J. Berkowitz and C. Lifshitz, J. Phys. B 1, 438 (1968); (c) R. B. Cairns, H. Harrison, and R. I. Schoen, J. Chem. Phys. 53, 96 (1970).

[18]Depolarization of angular correlations, owing to the lack of information about the orientation of unobserved angular momenta, is a concept that is central to the theory of angular correlation. See U. Fano and G. Racah, *Irreducible Tensorial Sets* (Academic, New York, 1959), Chap. 19, and especially p. 110, last paragraph.

[19]W. C. Martin, J. Sugar, and J. L. Tech, Phys. Rev. A 6, 2022 (1972) have verified the triplet character of this level using intermediate coupling theory with configuration interaction. They report that the $5d^9(^2D_{3/2})\,6s^2 6p_{3/2}$ ($J=1$, $\pi=-1$) level at 11.62 eV is composed of 63.3% $^3D_1^\circ$, and 29.5% $^3P_1^\circ$, the total singlet composition is less than 7%. These authors find substantial triplet character for many of the autoionizing levels of Hg [see also W. C. Martin, J. Sugar, and J. L. Tech, J. Opt. Soc. Am. 62, 1488 (1972)]. The deviation of β from 2 is evidence of this triplet character.

PHYSICAL REVIEW A VOLUME 7, NUMBER 6 JUNE 1973

Variational Calculations of Electron–Alkali-Metal-Atom Scattering: Elastic Scattering by Li, Na, and K†

A.-L. Sinfailam* and R. K. Nesbet
IBM Research Laboratory, San Jose, California 95193
(Received 14 February 1973)

Elastic total and spin-exchange cross sections are computed for electron scattering by Li, Na, and K, for energies below the first excitation threshold. The method used is the variational form of solution of continuum Bethe-Goldstone equations. Results are in substantial agreement with close-coupling calculations and with recent experimental data.

I. INTRODUCTION

This paper presents results of variational calculations of electron scattering by Li, Na, and K atoms in the low-energy region, below the n_0p excitation threshold for atomic ground-state configurations n_0s. The method has been described in sufficient detail elsewhere,[1] and will not be repeated here. Variational equations are solved equivalent to the continuum Bethe–Goldstone equation for the incident and series electrons in electron–alkali-metal-atom scattering.[2] The method is similar to that of Harris and Michels.[3] The specific variational formalism used here is the "optimized anomaly-free" (OAF) method.[4]

Detailed close-coupling calculations of low-energy-electron scattering by alkali-metal atoms have recently been published.[5,6] The present results, using quite different methodology, essentially confirm these close-coupling results, while providing a test of the new methods used here. Only the lowest-order phase shifts have been computed ($L=0$, 1, 2 for singlet and triplet states). The results obtained indicate that in the elastic scattering region higher-order phase shifts would simply duplicate results already obtained by close-coupling calculations or by the polarization formula used by Moores and Norcross for $L \geq 8$.

Theoretical and experimental results on electron–alkali-metal elastic scattering have been reviewed by Bederson.[7] Recent literature is discussed by Moores and Norcross.[6]

II. CHOICE OF BASIS FUNCTIONS

In a previous publication[1] we have described an investigation of the relative convergence properties of two methods of choosing basis functions for linear expansion of the variational wave function. Radial orbital basis functions are of the form

$$\phi_i = N r^{n-1} e^{-\zeta r} Y_{\ell m}(\theta, \phi)\ . \qquad (1)$$

With the $e^- + He$ problem as a test case, two methods of choosing basis functions were examined: (i) a sequence of exponents ζ in *decreasing* geometric progression for fixed n, complemented by an increasing arithmetic sequence of exponents for the same index n, (ii) a sequence of exponents ζ in *increasing* geometric progression for fixed n, complemented by a sequence with fixed ζ and increasing powers n. It can be shown that both methods